Journal of the Ceramic Society of Japan 118 [12] 1124-1130 2010 Special Article
The 64th CerSJ Awards for Academic Achievements in Ceramic Science and Technology: Review

Thin film processing of MoO_3 based hybrid materials

Ichiro MATSUBARA†

National Institute of Advanced Industrial Science and Technology, Shimo-Shidami, Moriyama-ku, Nagoya 463–8560

Intercalative inorganic–organic hybrids with useful properties have attracted much attention owing to their potential applications in various kinds of devices. The development of thin film process is crucial to realize a novel device using the hybrid materials. Thin films of the intercalated organic/MoO_3 hybrids have been prepared by an ex-situ intercalation process. The host MoO_3 films were first deposited on substrates by using a CVD method followed by the intercalation of organic components into the MoO_3 films. The preparation of highly *b*-axis oriented MoO_3 films is essential to prepare the organic/MoO_3 films. The organic/MoO_3 films show semiconducting-like transport. The organic/MoO_3 films show a distinct response to VOCs by changing their electrical resistivity and exhibit higher sensitivities to aldehyde gases, whereas almost no response to toluene and xylene. The VOC sensing performance is closely related to the microstructure of the organic/MoO_3 thin films, which is able to be controlled by the growth conditions of the host MoO_3 thin films.

Key-words : Thin films, Hybrid materials, Electrical properties, Intercalation, VOC sensors

[Received August 9, 2010; Accepted September 27, 2010]

1. Introduction

The Preparation of inorganic–organic hybrid materials has received considerable attention because of the prospect of developing materials with unique microstructures and properties.[1)–3)] The interesting point of such materials is the large numbers of chemical and structural modifications available. The inorganic–organic hybrid materials can be classified into four categories.[2),4)] The first one can be described as micro or nanocomposites in which one component (inorganic or organic) is dispersed in the other component that is acting as the host matrix. The second type consists of materials with covalent bonding between the two components, resulting in homogeneous hybrid materials at the molecular level. These materials are usually synthesized by co-polymerization of inorganic material precursors and organic monomers. The third type of hybrid materials can be described as organically modified inorganic materials. In general, such materials result from surface modification using coupling agents able to react with the hydroxy groups present on the metal oxide surface. The fourth hybrid materials are prepared by an intercalation reaction. Organic components are incorporated into the interlayer space of inorganic host materials with a layered structure.

We have focused on the intercalative hybrids with ordered stacking of inorganic and organic layers. The ordered structure can make it possible to design the materials by the concept of function shearing by both the components and harmonizing them in a nanoscale. The appropriate combination of both the components makes potential materials with both inorganic and organic characteristics.[5)] Advanced materials derived according to these principles have useful properties involving chemical sensors, field-effect transistors, light emitters, and batteries.[4),6)–9)] Although the intercalative hybrids have promising and unique properties, it has been hard to realize practical applications especially in the field of electronic functional materials because the reliable and reproducible thin film processing has not been established.

We have reported that organic/MoO_3 intercalative hybrids have semiconducting-type transport properties and exhibit selective response to aldehyde gases by changing their electrical resistivity, which is induced by the incorporation of the aldehyde molecules into the interlayers.[10)] From the viewpoint of sensor applications of organic/MoO_3, it is necessary to fabricate thin film devices. In the present review paper, preparation and volatile organic compound (VOC) sensing properties of organic/MoO_3 thin films are presented. We have fabricated organic/MoO_3 thin films by an ex-situ intercalation process.[11)–22)] The host MoO_3 films are first deposited by a CVD method followed by the intercalation of organic spices. Here, we report details of the preparation method and the VOC gas sensing properties of the organic/MoO_3 thin films.

2. Organic/MoO_3 hybrids

One of the most interesting properties of the orthorhombic MoO_3 is its intercalation ability. The structure of MoO_3 consists of vertex-sharing chains of distorted MoO_6 octahedra, which share edges with two similar chains to form layers. The two dimensionally bonded double-octahedra oxide sheets are stacked in a layered arrangement and are held together by weak van der Waals forces. Many organic components can be intercalated into the interlayers.[23)–27)] We have synthesized polypyrrole (PPy) intercalated MoO_3 hybrid material, $(PPy)_xMoO_3$ (**Fig. 1**), using a concomitant ion exchange reaction in a powder form. The $(PPy)_xMoO_3$ hybrid material was prepared by a two-step process.[10)] First, hydrated sodium ions were inserted into the MoO_3 layers ($[Na(H_2O)_5]_yMoO_3$) and then PPy was intercalated by ion exchange.

Temperature dependence of the resistivity (ρ) of $(PPy)_xMoO_3$ pressed pellets is shown in **Fig. 2**. The resistivity value of the pressed pellet is 9.6 Ω cm at room temperature, whereas pristine MoO_3 has a room temperature resistivity of 2×10^{10} Ω cm.[28)] Hole doped PPy is one of the typical conducting polymers and the electron doped MoO_3 should have a n-type semiconducting

† Corresponding author: I. Matsubara; E-mail: matsubara-i@aist.go.jp

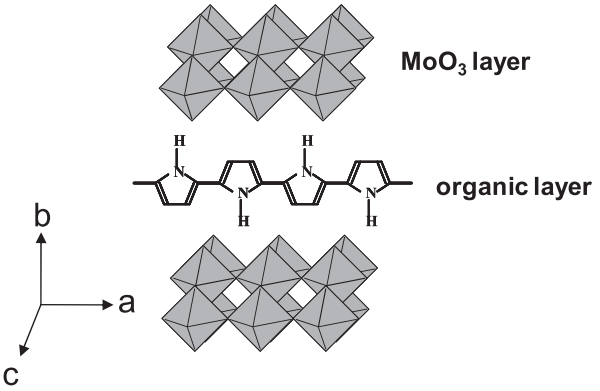

Fig. 1. Schematic illustration of the organic/MoO_3 structure.

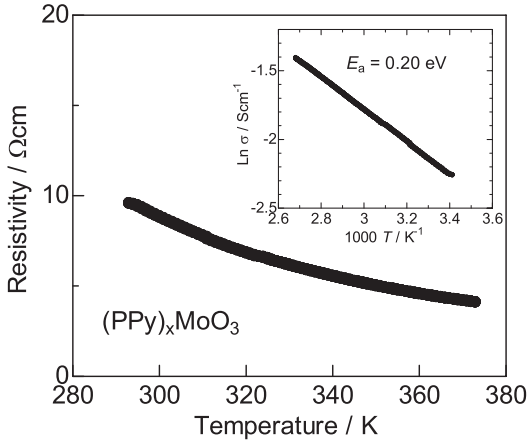

Fig. 2. Temperature dependence of resistivity of the $(PPy)_xMoO_3$ pressed pellet.

characteristics. Therefore, both the inorganic and organic layers become possible conducting path. Temperature dependence of resistivity of PPy is well described by the variable-range-hopping law, $\rho = \rho_0(T/T_0)^{1/2}\exp((T_0/T)^{1/4})$, where ρ_0 is a virtually temperature-independent material parameter and T_0 a measure for the degree of charge carrier localization.[29] As shown in Fig. 2, $(PPy)_xMoO_3$ shows a linear relationship in the ln (ρ) versus $1/T$ plot. The apparent activation energy is calculated to be 0.20 eV, which is consistent with that of polymer intercalated molybdenum oxides.[24] On the other hand, the activation energy of $(PPy)_xRuCl_3$ is 0.1 eV.[30] These comparisons imply that the MoO_3 host layers play a dominant role in determining transport properties of $(PPy)_xMoO_3$. Carrier electrons are transferred from the PPy layers to the MoO_3 layers in the $(PPy)_xMoO_3$.

The pressed pellets of the $(PPy)_xMoO_3$ powder show a distinct response to VOCs by increasing their electrical resistivity.[10] **Figure 3** shows room temperature response (R_g/R_a, where R_g and R_a are the electrical resistance in a test gas and air, respectively) of the $(PPy)_xMoO_3$ pressed pellets to various VOCs, formaldehyde, acetaldehyde, methanol, ethanol, chloroform, acetone, toluene, and benzene with the concentration of 1000 ppm. The $(PPy)_xMoO_3$ sample exhibits higher sensitivities to polar analytes, whereas it shows almost no response to toluene and benzene. The highest sensitivity was obtained for formaldehyde.

The $(PPy)_xMoO_3$ hybrid materials consist of alternately stacked negatively charged MoO_3 and positively charged PPy layers. The electrostatic interaction between the two layers is the

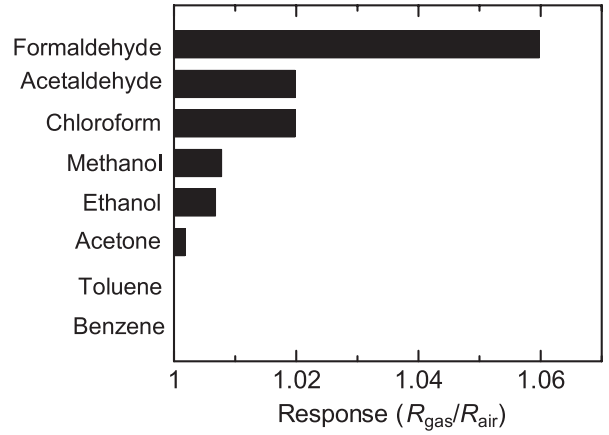

Fig. 3. The magnitude of the response (R_g/R_a) of $(PPy)_xMoO_3$ at a room temperature upon exposure of VOCs with the concentration of 1000 ppm.

main force to form the layered structure. In the $(PPy)_xMoO_3$, the PPy layers could be adsorption sites of VOC molecules. The affinities for positively charged PPy could induce the incorporation of the polar VOC molecules into the interlayers of $(PPy)_xMoO_3$. The insertion of the analyte VOC molecules may cause two effects on the conductivity. One is a physical effect due to the change in the interlayer distance of the layered materials, which could affect the degree of the charge transfer from PPy to MoO_3 layers, and hence the conductivity of the hybrid materials. The other is a partial charge transfer between the analyte VOC molecules and PPy. According to Josowicz et al., such the partial electron transfer may increase or reduce the concentration of the charge carriers in the polymer backbone.[31),32] The direction of the charge transfer is determined by the relative magnitude of the electronegativity of the analyte molecules and the work function of the polymer. The partial charge transfer affects the degree of the interlayer electron transfer from PPy to MoO_3 and then the conductivity of the hybrid materials.

3. Thin films of organic/MoO_3 hybrids

3.1 Preparation of organic/MoO_3 hybrid thin films

Because the vapor pressure and decomposition temperature of the inorganic and organic individual compound are too different, the intercalative inorganic–organic hybrid thin films cannot be prepared by the standard techniques such as sputtering, laser ablation, coevaporation, and CVD. The growth of intercalative inorganic–organic hybrid thin films has been achieved by several alternative methods. The most widely used technique is the delamination/reassembling process, in which the inorganic and organic components are piled up from a colloidal state onto a substrate.[33)–38] The thin films prepared by this method, however, have the problems of adhesion with the substrate, and the films are easily peeled off. Solution-based or evaporative thin-film techniques have been reported to prepare halide-based inorganic–organic perovskites.[39),40] Although high-quality thin films have been obtained, these techniques can be adopted only to halide-based perovskites and related hybrid materials.

We prepared $(PPy)_xMoO_3$ thin films by three-step process (**Fig. 4**).[11] First, MoO_3 thin films were prepared by CVD on $LaAlO_3$ (LAO) single crystal and LAO/Si substrates. The intercalation of PPy was carried out by the method as in the case of the powder sample. The MoO_3 thin films were immersed

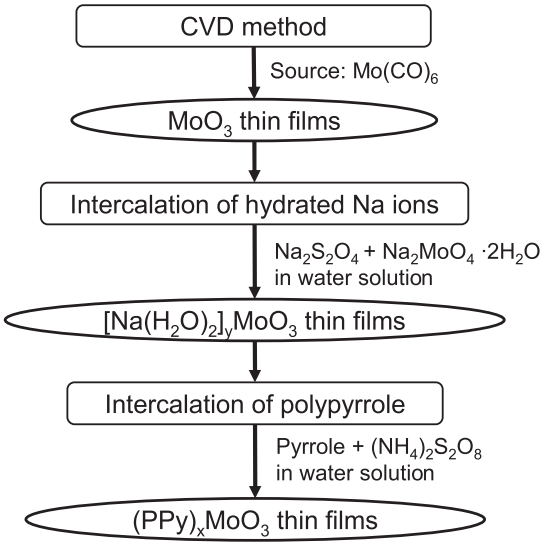

Fig. 4. Flowchart for the preparation of $(PPy)_xMoO_3$ hybrid thin films.

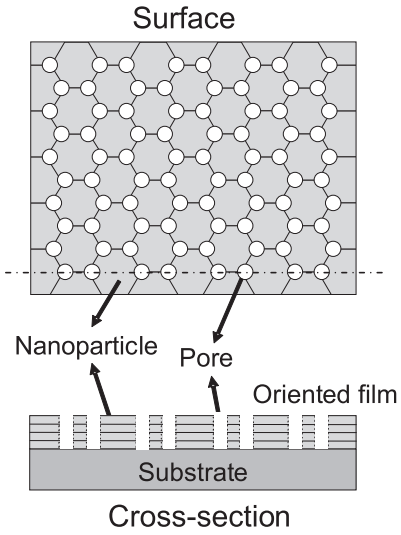

Fig. 5. Schematic drawing of the microstructure necessary for hybrid thin films with high VOC sensing performance.

in an aqueous solution of $Na_2S_2O_4$ to obtain $[Na(H_2O)_2]_yMoO_3$ thin films. The hydrated sodium ions intercalated MoO_3 thin films were next immersed in a PPy aqueous solution for the ion exchange reaction to give the $(PPy)_xMoO_3$ thin films.

3.2 Control the microstructure of organic/MoO_3 hybrid thin films

The key point in the process of the organic/MoO_3 hybrid thin films is the deposition of MoO_3 thin films from the view point of controlling the microstructure of the hybrid thin films. There are three important factors to be considered in the MoO_3 thin film microstructures, small grain size, porous structure, and high *b*-axis orientation. The hybrid thin films should have a porous structure consisting of nano size grains in order to achieve a high sensitivity to VOCs. Because the sensor response is induced by the incorporation of the analyte VOC molecules into the organic layers, a porous structure improving the interaction between the hybrid materials and VOC molecules is required. The small grain size can increase the specific surface area of the thin films and enhance the effective interaction between the hybrid materials and the analyte VOC molecules. The third factor, high orientation, is important to fabricate the hybrid thin films with such the microstructure without peeling the films from the substrate during the intercalation process. The intercalation of hydrated sodium ions expands the interlayer spacing by 0.28 nm compared to MoO_3, indicating that $[Na(H_2O)_2]^+$ units are incorporated into the MoO_3 layers. After the ion exchange reaction, the intercalated PPy expands the interlayer spacing of the MoO_3 lattice along the *b*-axis more. The interlayer spacing of $(PPy)_xMoO_3$ is equal to 1.47 nm, corresponding to an interlayer expansion of 0.78 nm compared to the MoO_3, sufficient to accommodate the PPy molecules. When the host MoO_3 films have a random orientation, the films could be peeled off due to the strain generated by the interlayer expansion. In the case of highly *b*-axis oriented MoO_3 films, since the strain is generated only in the out-of-plane direction, the peeling problem could be avoided. Highly *b*-axis oriented MoO_3 films are, therefore, necessary to prepare $(PPy)_xMoO_3$ thin films in this ex-situ intercalation process.

Figure 5 shows the required microstructure of the organic/MoO_3 hybrid thin films. As the intercalation reaction proceeds without changing the microstructure of the MoO_3 host thin films, the controlled growth of the MoO_3 thin films are essential to achieve the required microstructure in the organic/MoO_3 hybrid thin films. MoO_3 thin films have been reported to be prepared by various techniques such as CVD,[41),42)] sputtering,[43)] flash and thermal deposition,[44)] electrodeposition,[45)] and hot-filament deposition.[46)] Here we adopted a CVD technique using a solid molybdenum source, $Mo(CO)_6$.[11)] As a high vacuum environment is not necessary to deposit the films by this method, the orthorhombic MoO_3 phase is formed in the as-grown films without post annealing. Another advantageous point is a higher deposition rate to form the MoO_3 thin films of substantial thickness.

The host MoO_3 thin films were prepared on LAO and MgO single crystal substrates.[11)] The XRD pattern of the MoO_3 thin films on LAO single crystal exhibits the dominant *b*-axis orientation. On the other hands, the MoO_3 thin films on MgO single crystal have a poor *b*-axis orientation compared with that on LAO. The *a*- and *c*-axis lengths of the orthorhombic MoO_3 have been reported to be 0.3963 nm and 0.3696 nm, respectively.[47)] The in-plane average length of the *a*- and *c*-axis is 0.3830 nm. The *a*-axis length of LAO and MgO are 0.3790 nm and 0.4216 nm, respectively. The lattice mismatch between MoO_3 and the substrate is calculated to be 1.03% and 9.97% for LAO and MgO, respectively. The poor *b*-axis orientation observed for the MgO substrate is due to the large lattice mismatch. The choice of an appropriate substrate is crucial to obtain highly *b*-axis oriented MoO_3 thin films.

Form the view point of the practical application of the organic/MoO_3 hybrid thin films as VOC sensors, inexpensive substrates instead of LAO single crystals are required to fabricate low-cost devices. We have tried to adopt Si as the substrate for the hybrid thin films.[14)] The LAO buffer layer is formed on the silicon wafer with thermally oxidized SiO_2 insulating layer. The LAO-coated silicon substrate was prepared by a spin coating method using LAO source solution. The LAO buffer layer works well to form the oriented MoO_3 thin films on it. When we use Si substrates without the buffer layer, the films are peeled off during the intercalation process.

In order to realize the target microstructure shown in Fig. 5, the growth mechanism of the MoO_3 thin films by the CVD

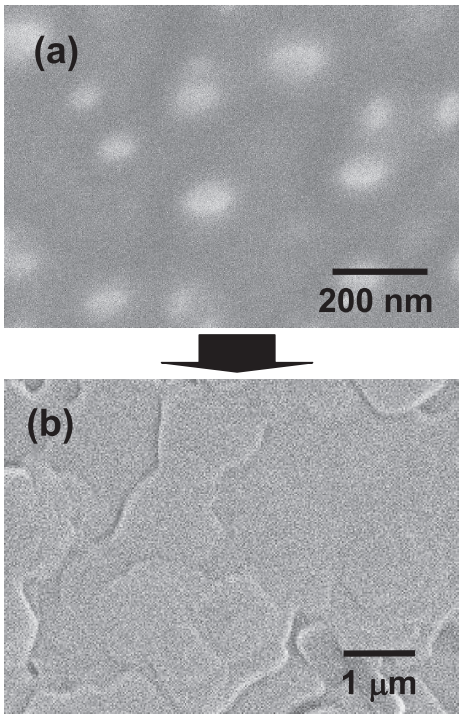

Fig. 6. Surface morphology of the MoO_3 thin films deposited on LAO substrate for (a) 10 s and (b) 15 min.

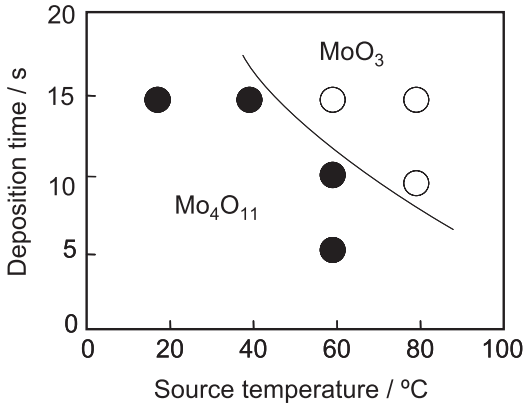

Fig. 7. Relationship between the growth phase and the deposition conditions at the early stage of the MoO_3 thin film growth.

method has been investigated. **Figure 6** shows the surface morphology of the thin films deposited on LAO single crystal substrate for 10 s (Fig. 6(a)) and 15 min (Fig. 6(b)) at the substrate temperature of 480°C. At the early stage of the film growth, the islands of MoO_3 are observed, and they grow to cover hole the substrate, and then well oriented MoO_3 thin films are obtained. The growth phase of the early stage depends on the deposition time and source temperature. The impurity phase of Mo_4O_{11} is detected by XRD in the conditions of a low source temperature and a short deposition time as shown in **Fig. 7**. From this result, we have determined the source temperature for the MoO_3 thin film growth. Another important factor for controlling the microstructure of the MoO_3 thin films is the substrate temperature. **Figure 8** shows the surface morphology of the MoO_3 thin films deposited at the substrate temperature from 440 to 500°C. The source temperature and deposition time were fixed

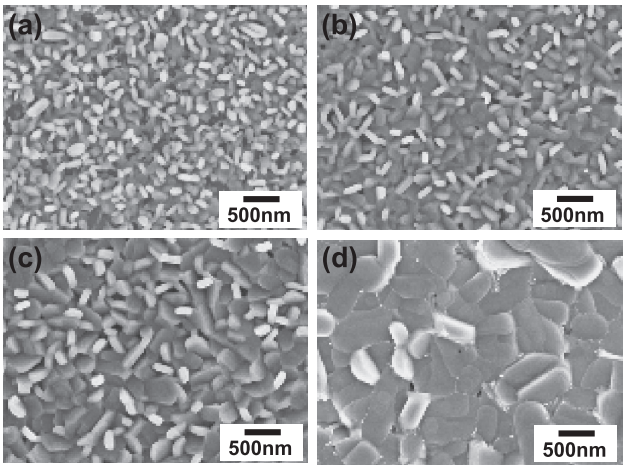

Fig. 8. Scanning electron micrographs of MoO_3 thin films on LAO/Si deposited at (a) 440, (b) 460, (c) 480, and (d) 500°C.

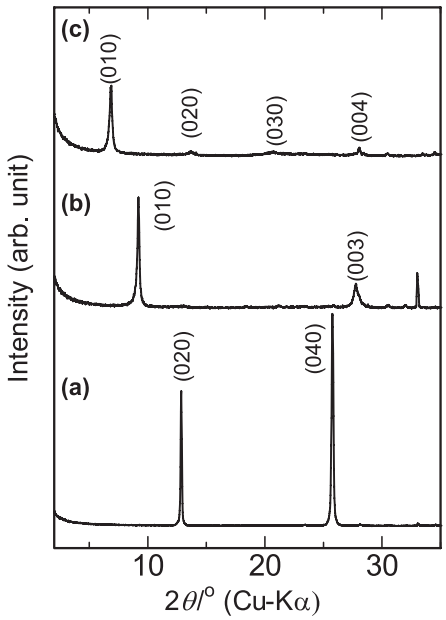

Fig. 9. X-ray diffraction patterns of (a) MoO_3, (b) $[Na(H_2O)_2]_yMoO_3$, and (c) $(PANI)_xMoO_3$ thin films.

at 60°C and 15 min, respectively. The film thickness is around 200 nm. The grain size was increased with increasing the substrate temperature from several tens to several hundreds of nm. Porous structure with nano size grains is appeared to be formed in the film deposited at 440°C (Fig. 8(a)). However, when this film was applied to the intercalation process, the film was peeled off due to the week adhesion between the film and the substrate. This problem was not observed for the other films deposited at higher substrate temperatures. By using the MoO_3 thin films deposited at 460°C, we obtained the organic/MoO_3 hybrid thin films with keeping the microstructure of the MoO_3 thin films. By the ex-situ intercalation process, we are able to control the microstucture of the organic/MoO_3 thin films.

XRD patterns of polyaniline (PANI) intercalated MoO_3, $[Na(H_2O)_2]_yMoO_3$, and MoO_3 thin films are shown in **Fig. 9**.[13] PANI is also intercalated into the MoO_3 layers by ion exchange method as in the case of PPy. It is noted that the *b*-axis diffraction peaks dominate the diffraction pattern, with four observed (0k0)

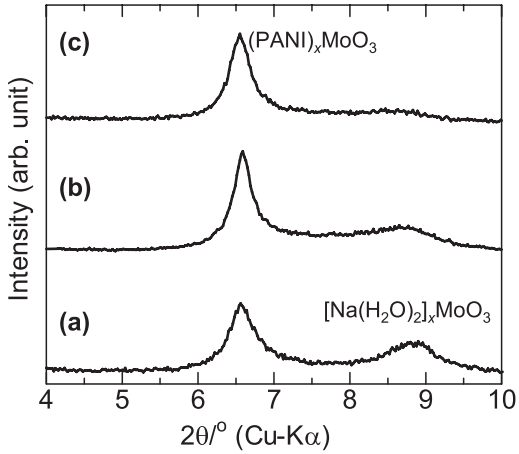

Fig. 10. X-ray diffraction patterns of $(PANI)_xMoO_3$ crystals with different intercalation reaction time, (a) 10, (b) 20, and (c) 30 min.

peaks. The presence of higher order peaks indicates that the formed $(PANI)_xMoO_3$ film is well-ordered. The interlayer distance of $(PANI)_xMoO_3$ (0.64 nm) is in agreement with the molecular size of the benzene ring, indicating nearly perpendicular orientation of PANI chains to the MoO_3 sheets. In the XRD pattern of the $(PANI)_xMoO_3$ thin film, no MoO_3 and $[Na(H_2O)_2]_yMoO_3$ phases remain, indicating that the intercalation of PANI successfully proceeds in the present process. The intercalation reaction of PANI to form the $(PANI)_xMoO_3$ thin films is completed within 30 s, which is much shorter than that for single crystals. **Figure 10** shows the change of the XRD pattern during the intercalation reaction for MoO_3 single crystals prepared by a flux method. The size of the MoO_3 single crystals is 0.5–3 mm in length, 0.2–0.5 mm in width, and 30–80 μm in thickness. $[Na(H_2O)_2]_yMoO_3$ crystals were prepared by the same method as in the case of the powder samples. During the intercalation of PANI, $[Na(H_2O)_2]_yMoO_3$ phase remain for the reaction time less than 30 min. The fast intercalation reaction observed in the thin films should be due to the small grain size and porous structure. Such the microstructure is also preferable from the view point of the intercalation reaction.

3.3 VOC gas sensing properties

The gas sensing properties of the $(PANI)_xMoO_3$ thin films to formaldehyde and acetaldehyde gases were evaluated.[20] Air and a ppb level aldehyde/air mixture gas were alternatively flowed into a measurement chamber. Upon exposure to formaldehyde and acetaldehyde gases, the electrical resistance increased. When the supply of the gas stopped, the resistance value returned to almost the original one. The $(PANI)_xMoO_3$ thin films exhibit the distinct response even to 25 ppb formaldehyde and acetaldehyde gases by increasing its electrical resistance. We also measured the response to various VOCs methanol, ethanol, chloroform, acetone, toluene, and xylene. The resistance increasing response was obtained for formaldehyde and acetaldehyde gases. On the other hand, no response was obtained to the other VOC gases. The selective detection with high sensitivity to aldehyde gases is achieved in the $(PANI)_xMoO_3$ thin films.

One of the most interesting points of the MoO_3 based hybrid materials is the flexibility for selecting the organic component. In the case of $(PANI)_xMoO_3$ and $(PPy)_xMoO_3$, the response to aldehyde gases is induced by the incorporation of gas molecules into the organic layers. Therefore, the sensor response should

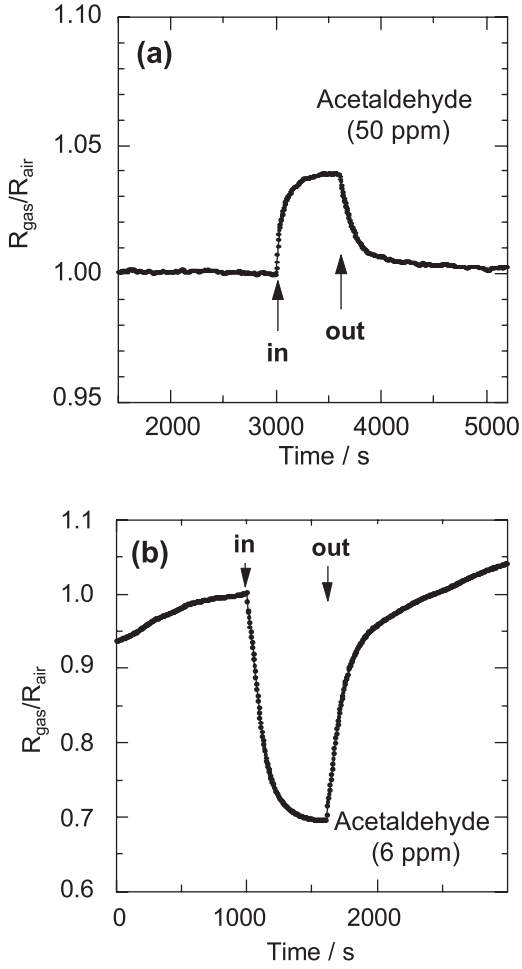

Fig. 11. Dynamic response of the (a) $(PANI)_xMoO_3$ and (b) $(PS)_x(C_{26}H_{56}N)_yMoO_3$ thin films to acetaldehyde.

depend on the kind of the organic component. By the above described method, we have prepared various kinds of organic/MoO_3 hybrid thin films and systematically evaluated the sensing properties to VOCs. The organic components used in this study are PANI, PANI derivatives (Poly(dimethylaniline),[16] poly-(N-methylaniline),[17] Poly(o-anisidine),[18] poly(5,6,7,8-tetrahydro-1-naphthylamine)[19]), PPy, PPy derivatives, polythiophene derivatives, polystylene (PS) with surfactant,[13] porphyrin derivatives (5,10,15,20-tetrakis(N-methyl-4-pyridino) porphyrin,[21] and alkyl ammonium salts.[12]

The sensitivity and selectivity to VOCs depend on the kind of the organic component, indicating that the organic layers act as molecular recognition. The $(PPy)_xMoO_3$ and $(PANI)_xMoO_3$ thin films exhibit a response to formaldehyde and acetaldehyde gases by increasing their electrical resistance. However, the PS and surfactant intercalated $(PS)_x(C_{26}H_{56}N)_yMoO_3$ thin films exhibit a reverse response.[13] **Figure 11** shows the dynamic response of the $(PANI)_xMoO_3$ and $(PS)_x(C_{26}H_{56}N)_yMoO_3$ thin films to acetaldehyde gas with a concentration of 50 ppm and 6 ppm, respectively, balanced with nitrogen at 45°C. The response value of the $(PS)_x(C_{26}H_{56}N)_yMoO_3$ thin film is around $R_a/R_g = 1.3$, which is much higher than that of the $(PANI)_xMoO_3$. The $(PS)_x(C_{26}H_{56}N)_yMoO_3$ thin films exhibit a similar resistance decreasing response to formaldehyde. In the case of $(PANI)_xMoO_3$, the aldehyde gas molecules could dominantly interact with the organic species, which could reduce the

interlayer charge transfer from the organic to the MoO_3 layers. The effective carrier density is, thierefore, reduced and the resistance increasing response can be observed. On the other hand, when the $(PS)_x(C_{26}H_{56}N)_yMoO_3$ with a large interlayer spacing are exposed to analyte vapors such as formaldehyde and acetaldehyde, the gas molecules could dominantly interact with the specific surfaces of the charged MoO_3 layers compared with the hydrophobic layers. In the large space in the gallery of MoO_3 host, an unshared electron pair of an oxygen atom of the molecule of aldehyde (–CHO:) is pulled into a vacant *d*-orbital of the surface Mo^{6+} cation.[48] In this situation, extra charge could supply to MoO_3 and resistance decreasing response should be observed due to the increasing of carrier density.

4. Conclusion

The organic/MoO_3 hybrid thin films have been prepared by an ex-situ intercalation process. The host MoO_3 films were first deposited on substrates by using a CVD method followed by the intercalation of organic components. The microstructure of the organic/MoO_3 hybrid thin films can be controlled by the growth conditions of the host MoO_3 thin films. The organic/MoO_3 hybrid thin films exhibit a high sensitive and selective response to aldehyde gases by changing their electrical resistivity. The development of the thin film process makes it possible to apply the organic/MoO_3 hybrids in VOC sensor devices. The ex-situ intercalation process could be adapted to other intercalative inorganic–organic hybrids with unique properties.

Acknowledgements The author would like to express his sincerest gratitude to all the coauthors and collaborators. This work was partially supported by New Energy and Industrial Technology Development Organization (NEDO).

References

1) U. Schubert, N. Husing and A. Lorenz, *Chem. Mater.*, 7, 2010–2027 (1995).
2) C. Sanchez and F. Ribot, *New J. Chem.*, 18, 1007–1047 (1994).
3) M. Ogawa and K. Kuroda, *Chem. Rev.*, 95, 399–438 (1995).
4) C. Guizard, A. Bac, M. Barboiu and N. Hovnanian, *Sep. Purif. Methods*, 25, 167–180 (2001).
5) J. H. Harreld, B. Dunn and L. F. Nazar, *Int. J. Inorg. Mater.*, 1, 135–146 (1999).
6) A. Walcarius, *Chem. Mater.*, 13, 3351–3372 (2001).
7) C. R. Kagan, D. B. Mitzi and C. D. Dimitrakopoulos, *Science*, 286, 945–947 (1999).
8) L. Sheeney-Haj-Ichia, J. Wasserman and I. Willner, *Adv. Mater.*, 14, 1323–1326 (2002).
9) K. Tsure, S. Hayakawa, C. Ohtsuki and A. Osaka, *J. Sol-Gel Sci. Technol.*, 13, 237–240 (1998).
10) I. Matsubara, N. Murayama, W. Shin, N. Izu and K. Hosono, *Bull. Chem. Soc. Jpn.*, 77, 1231–1237 (2004).
11) K. Hosono, I. Matsubara, N. Murayama, W. Shin and N. Izu, *Chem. Mater.*, 17, 349–354 (2005).
12) I. Matsubara, N. Murayama, W. Shin and N. Izu, Mater. Res. Soc. Symp. Proc. 2004 Fall Meeting, Vol. 847 (2005) pp. 249–254.
13) J. Wang, I. Matsubara, N. Murayama, W. Shin and N. Izu, *Thin Solid Films*, 514, 329–333 (2006).
14) T. Itoh, I. Matsubara, W. Shin and N. Izu, *Thin Solid Films*, 515, 2709–2716 (2006).
15) J. Wang, I. Matsubara, T. Itoh, N. Murayama, W. Shin and N. Izu, *IEEJ Trans. SM*, 126, 548–552 (2006).
16) T. Itoh, I. Matsubara, N. Murayama, W. Shin and N. Izu, *Chem. Lett.*, 36, 100–101 (2007).
17) T. Itoh, I. Matsubara, W. Shin and N. Izu, *Mater. Lett.*, 61, 4031–4034 (2007).
18) T. Itoh, I. Matsubara, W. Shin and N. Izu, *Bull. Chem. Soc. Jpn.*, 80, 1011–1016 (2007).
19) T. Itoh, I. Matsubara, W. Shin, N. Izu and M. Nishibori, *J. Ceram. Soc. Japan*, 115, 742–744 (2007).
20) T. Itoh, I. Matsubara, W. Shin, N. Izu and M. Nishibori, *Sens. Actuators, B*, 128, 512–520 (2008).
21) T. Itoh, J. Wang, I. Matsubara, W. Shin, N. Izu, M. Nishibori and N. Murayama, *Mater. Lett.*, 62, 3021–3023 (2008).
22) I. Matsubara, T. Itoh, W. Shin, N. Izu and M. Nishibori, *Adv. Mater. Res.*, 47–50, 1514–1517 (2008).
23) T. A. Kerr, H. Wu and L. F. Nazar, *Chem. Mater.*, 8, 2005–2015 (1996).
24) L. F. Nazar, Z. Zhang and D. J. Zinkweg, *J. Am. Chem. Soc.*, 114, 6239–6240 (1992).
25) G. R. Goward, T. A. Kerr, W. P. Power and L. F. Nazar, *Adv. Mater.*, 10, 449–452 (1998).
26) N. Sukpirom, C. O. Oriakhi and M. M. Lerner, *Mater. Res. Bull.*, 35, 325–331 (2000).
27) K. Shao, Y. Ma, Y. Cao, Z. Chen, X. Ji and J. Yao, *Chem. Mater.*, 13, 250–252 (2001).
28) N. Kumagai and K. Tanno, *J. Appl. Electrochem.*, 18, 857–862 (1988).
29) K. K. Kanazawa, A. F. Diaz, W. D. Gill, P. M. Grant, G. B. Street and G. P. Gardini, *Synth. Met.*, 1, 329–336 (1980).
30) L. Wang, M. Rocci-Lane, P. Brazis, C. R. Kannewurf, Y. I. Kim, W. Lee, J. H. Choy and M. G. Kanatzidis, *J. Am. Chem. Soc.*, 122, 6629–6640 (2000).
31) D. Blackwood and M. Josowicz, *J. Phys. Chem.*, 95, 493–502 (1991).
32) P. Topart and M. Josowicz, *J. Phys. Chem.*, 96, 7824–7830 (1992).
33) Z. H. Liu, X. J. Yang, Y. Makita and K. Ooi, *Chem. Mater.*, 14, 4800–4806 (2002).
34) L. Wang, Y. Omomo, N. Sakai, K. Fukuda, I. Nakai, Y. Ebina, K. Takada, M. Watanabe and T. Sakai, *Chem. Mater.*, 15, 2873–2878 (2003).
35) B. B. Lakshmi, P. K. Dorhout and C. R. Martin, *Chem. Mater.*, 9, 857–862 (1997).
36) J. H. Choy, S. M. Paek, J. M. Oh and E. S. Jang, *Curr. Appl. Phys.*, 2, 489–495 (2002).
37) N. Sukpirom and M. M. Lerner, *Mater. Sci. Eng., A*, 354, 180–187 (2003).
38) T. Malzbender and G. de With, *Thin Solid Films*, 386, 68–78 (2001).
39) D. B. Mitizi, Synthesis, Structure, and Properites of Organic-Inorganic Perovskites and Related Materials, in "Progress in Inorganic Chemistry," Vol. 48, John Wiley & Sons, Inc., New York (1999).
40) D. B. Mitzi, M. T. Prikas and K. Chondroudis, *Chem. Mater.*, 11, 542–544 (1999).
41) T. Ivanova, A. Szekeres, M. Gartner, D. Gogova and K. A. Gesheva, *Electrochim. Acta*, 46, 2215–2219 (2001).
42) T. Ivanova, M. Surtchev and K. Gesheva, *Mater. Lett.*, 53, 250–257 (2002).
43) J. Scarminio, A. Lourenco and A. Gorenstein, *Thin Solid Films*, 302, 66–70 (1997).
44) C. Julien, G. A. Nazri, J. P. Guesdon, A. Gorenstein, A. Khelfa and O. M. Hussain, *Solid State Ionics*, 73, 319–326 (1994).
45) A. Guerfi and L. H. Dao, *J. Electrochem. Soc.*, 136, 2435–2436 (1989).
46) M. A. Bica de Moraes, B. C. Trasferetti, F. P. Rouxinol, R. Landers, S. F. Durrant, J. Scarmínio and A. Urbano, *Chem. Mater.*, 16, 513–520 (2004).
47) X. M. Wei and H. C. Zeng, *J. Phys. Chem. B*, 107, 2619–2622 (2003).
48) U. Tritthart, A. Gavrilyuk and W. Gey, *Solid State Commun.*, 105, 653–657 (1998).

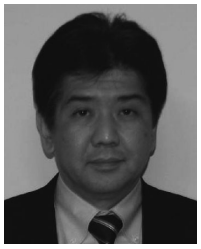

Ichiro Matsubara received his BS and MS degrees in polymer chemistry from Osaka University in 1985, 1987, respectively, and his doctorate of science degree in inorganic and physical chemistry from Osaka University in 1994. He is currently the leader of Electroceramics Process Group at Advance Manufacturing Research Institute, AIST, Japan. His research interests include inorganic–organic hybrid materials, functional oxide materials, and their sensor application.